IEEE Transactions on Energy Conversion, Vol. EC-2, No. 1, March 1987

A NEW LONGITUDINAL END EFFECT FACTOR FOR LINEAR INDUCTION MOTORS

J. F. Gieras
Member IEEE

G. E. Dawson
Member IEEE

A. R. Eastham
Senior Member IEEE

Department of Electrical Engineering
Queen's University
Kingston, Ontario, Canada K7L 3N6

Abstract - The longitudinal end effect in a linear induction motor (LIM) is analysed assuming two travelling magnetic flux density waves in the airgap: the wave travelling with synchronous velocity and the wave representing end effect [1]. A simple equation for the end effect factor which modifies the airgap EMF is obtained, and a simple equivalent circuit incorporating the end effect factor is established. Analysis is compared with measurements from two large-scale single-sided LIM's. The equation for the end effect factor is sufficiently accurate to be used for design studies of LIMs. Since end effects are negligible at low speeds, the end effect factor has application for medium and high-speed LIMs.

1. Formulation of Problem

The longitudinal end effect in linear induction motors is caused by the following factors:

(a) the finite length of the laminated primary stack and the abrupt change in the airgap magnetic reluctance at both ends of the machine;

(b) the consequent velocity-dependent nonuniformity of the secondary induced current distribution and of the airgap flux distribution along the length of the machine.

According to hypothesis and research conducted in Japan [1,2,3], the longitudinal end effect can be interpreted as a superposition of two travelling airgap magnetic flux density waves:

$$b(x,t) = B_{ms}\sin(\omega t - \frac{\pi}{\tau}x) + B_{me}e^{-\frac{x}{T_e}}\sin(\omega t - \frac{\pi}{\tau_e}x + \delta) \quad (1)$$

where B_{ms} is the peak value of the wave travelling with synchronous velocity $v_s = 2\tau f$, and B_{me} is the peak value of a damped entry-end wave travelling in the positive x direction with the velocity $v_{end} = 2\tau_e f$, as in Fig. 1. The pole pitch for the wave travelling with synchronous velocity is τ and is constant. The pole pitch for the entry-end-wave is τ_e and is dependent on operating conditions. At the front end of the machine, the entry-end wave is shifted in phase by an angle δ from the wave moving at synchronous velocity, and the attenuation constant for this wave is T_e. The phase angle is $\delta = \delta_1 - \delta_s$ according to Yamamura [1], pg 53. Both waves induce an EMF in the primary winding, as follows:

$$e = e_s + e_e = -E_{ms}\cos\omega t - E_{me}\cos\omega t \quad (2)$$

where e_s and E_{ms} are related to B_{ms}, and e_e and E_{me} are

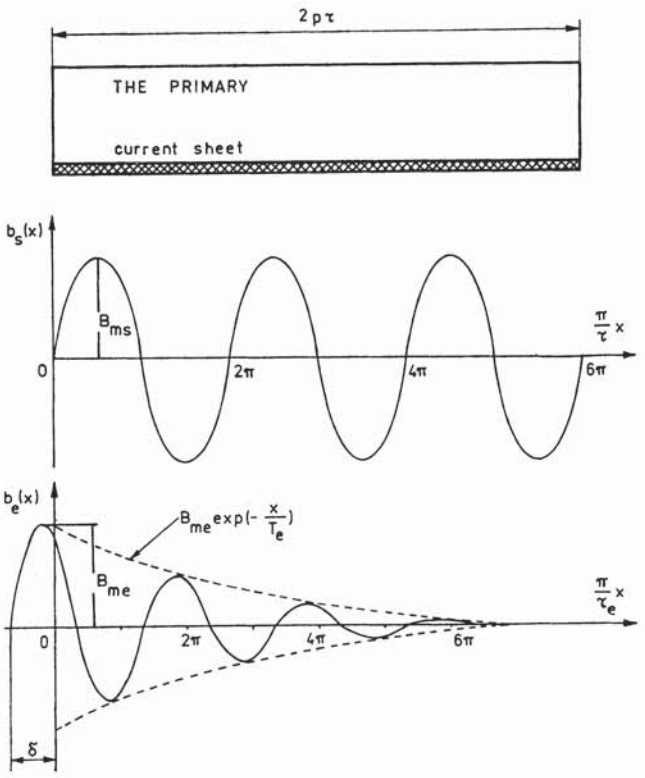

Fig. 1 The synchronous $B_{ms}\sin(\frac{\pi}{\tau}x)$ wave and the entry end effect $B_{me}e^{-\frac{x}{T_e}}\sin(\frac{\pi}{\tau_e}x + \delta)$ wave for $\tau_e \leq \tau$

86 WM 209-1 A paper recommended and approved by the IEEE Rotating Machinery Committee of the IEEE Power Engineering Society for presentation at the IEEE/PES 1986 Winter Meeting, New York, New York, February 2 - 7, 1986. Manuscript submitted September 5, 1984; made available for printing November 7, 1985.

0885-8969/87/0300-0152$01.00©1987 IEEE

related to B_{me}. The end effect factor is established according to the equation:

$$e = - E_{ms}(1 - k_e)\cos\omega t \qquad (3)$$

or

$$k_e = \frac{E_{me}}{E_{ms}} \qquad (4)$$

2. Assumptions

The following assumptions are used in our analysis to derive an analytical expression for k_e:

(a) the end effect wave is effectively equal to zero after the distance $2p\tau_e$, i.e. it induces airgap EMF only within the distance $0 \leq x \leq 2p\tau_e$,

(b) all magnetic and electric quantities vary sinusoidally with time,

(c) for speeds up to v_o, where $0 \leq v_o < v_s$, the end effect wave induces no voltage in the primary winding,

(d) in the limit $T_e \to \infty$ and $\tau_e = \tau$, the entry-end-effect wave cancels the wave travelling with synchronous velocity, i.e. $B_{me} = B_{ms}$,

(e) the flux linkage for each phase is the same.

The end effect wave is strongly damped along the x axis [1,4], so that assumption (a) will always be valid in practice.

Although, according to assumption (b), all quantities are considered to be sinusoidally time-dependent, the developed formulas for magnetic flux and EMF will be valid for nonsinusoidal time-dependence if one puts the appropriate form factors for the EMF and for the ratio of the average to the peak value of magnetic flux density. For sinusoidal waveforms, these factors are $\pi/(2\sqrt{2})$ and $2/\pi$ respectively.

There is no observed end effect influence on LIM performance for low speeds [1,4] - assumption (c). Assumption (d) represents a limiting condition, and is used to establish an analytical boundary condition. Assumption (e) establishes the same induced EMF in each phase winding.

The pole pitch $\tau_e > \tau$, in case of low-speed motors, implies that the end effect wave travels faster than the wave moving with synchronous velocity. According to Yamamura [1], a positive thrust is then produced at synchronous speed. This effect has been confirmed experimentally [5,6], though the magnitude of the positive thrust at zero slip is very small. In many cases, e.g. [7], this positive thrust is counteracted both by mechanical power losses and by a negative thrust due to higher space harmonics. For both designers and users of LIMs, negative forces due to end effect in intermediate and high speed LIMs are much more important than the small positive thrust for $\tau_e > \tau$ in some low-speed LIMs. Thus, this positive thrust will be neglected in analysis of the end effect factor.

3. EMF Due To Magnetic Flux Density Wave Travelling With Synchronous Velocity

The instantaneous value of airgap EMF per phase of the LIM, with stack width L and with effective number of turns per phase Nk_w, is equal to:

$$e_s = - pN_p k_w L \frac{d}{dt}\{[\int_o^{\tau} B_{ms} \sin\frac{\pi}{\tau}x \, dx] \sin\omega t\}$$

$$= - 2\pi f N k_w \frac{2}{\pi} \tau L B_{ms} \cos\omega t = - E_{ms}\cos\omega t \qquad (5)$$

where p = number of pole pairs, N_p = number of turns per pole pair per phase, N = number of turns per phase, k_w = winding factor, f = input frequency, E_{ms} = peak value of EMF induced by magnetic flux density moving with synchronous velocity.

4. EMF Due To End Effect Magnetic Flux Density Wave

Because the end effect magnetic flux density wave is damped along the x axis, Fig. 1, the magnetic flux per pole is different in each interval corresponding to the half wavelength τ_e. For the intervals $(2k-2)\tau_e \leq x \leq (2k-1)\tau_e$, where $k = 1,2,3,\ldots$, the following values of magnetic flux per pole can be established using assumption (b):

(i) for k = 1 (i.e. the first pole):

$$\Phi_{e1} = L B_{me} \sin\omega t \int_o^{\tau_e} e^{-\frac{x}{T_e}} \sin\left(\frac{\pi}{\tau_e}x + \delta\right) dx$$

$$= \frac{L B_{me} \sin\omega t}{\frac{1}{T_e^2} + \left(\frac{\pi}{\tau_e}\right)^2}\left(1 + e^{-\frac{\tau_e}{T_e}}\right) \cdot f(\delta)$$

(ii) for k = 2 (i.e. the third pole):

$$\Phi_{e3} = L B_{me} \sin\omega t \int_{2\tau_e}^{3\tau_e} e^{-\frac{x}{T_e}} \sin\left(\frac{\pi}{\tau_e}x + \delta\right) dx$$

$$= \frac{L B_{me} \sin\omega t}{\frac{1}{T_e^2} + \left(\frac{\pi}{\tau_e}\right)^2}\left(e^{-\frac{2\tau_e}{T_e}} + e^{-\frac{3\tau_e}{T_e}}\right) \cdot f(\delta)$$

$$\vdots$$

(iii) for k = p (i.e. the penultimate pole):

$$\Phi_{e2p-1} = L B_{me} \sin\omega t \int_{(2p-2)\tau_e}^{(2p-1)\tau_e} e^{-\frac{x}{T_e}} \sin\left(\frac{\pi}{\tau_e}x + \delta\right) dx$$

$$= \frac{L\,B_{me}\,\sin\omega t}{\frac{1}{T_e^2} + \left(\frac{\pi}{\tau_e}\right)^2}\left[e^{-\frac{(2p-2)\tau_e}{T_e}} + e^{-\frac{(2p-1)\tau_e}{T_e}}\right] \cdot f(\delta)$$

where $$f(\delta) = \frac{1}{T_e}\sin\delta + \frac{\pi}{\tau_e}\cos\delta \qquad (6)$$

On the other hand, for the intervals $(2k-1)\tau_e \leq x \leq 2k\tau_e$, where $k = 1,2,3, \ldots\ldots$, the following values of magnetic flux per pole can be established using assumption (b):

(i) for k = 1 (i.e. the second pole)

$$\Phi_{e2} = L\,B_{me}\,\sin\omega t \int_{\tau_e}^{2\tau_e} e^{-\frac{x}{T_e}} \sin\left(\frac{\pi}{\tau_e}x + \delta\right) dx$$

$$= -\frac{L\,B_{me}\,\sin\omega t}{\frac{1}{T_e^2} + \left(\frac{\pi}{\tau_e}\right)^2}\left(e^{-\frac{\tau_e}{T_e}} + e^{-\frac{2\tau_e}{T_e}}\right) \cdot f(\delta)$$

(ii) for k = 2 (i.e. the fourth pole)

$$\Phi_{e4} = L\,B_{me}\,\sin\omega t \int_{3\tau_e}^{4\tau_e} e^{-\frac{x}{T_e}} \sin\left(\frac{\pi}{\tau_e}x + \delta\right) dx$$

$$= -\frac{L\,B_{me}\,\sin\omega t}{\frac{1}{T_e^2} + \left(\frac{\pi}{\tau_e}\right)^2}\left(e^{-\frac{3\tau_e}{T_e}} + e^{-\frac{4\tau_e}{T_e}}\right) \cdot f(\delta)$$

$\vdots$

(iii) for k = p (i.e. the last pole)

$$\Phi_{e2p} = L\,B_{me}\,\sin\omega t \int_{(2p-1)\tau_e}^{2p\tau_e} e^{-\frac{x}{T_e}} \sin\left(\frac{\pi}{\tau_e}x + \delta\right) dx$$

$$= -\frac{L\,B_{me}\,\sin\omega t}{\frac{1}{T_e^2} + \left(\frac{\pi}{\tau_e}\right)^2}\left[e^{-\frac{(2p-1)\tau_e}{T_e}} + e^{-\frac{2p\tau_e}{T_e}}\right] \cdot f(\delta)$$

From a physical point of view (flux being continuous), it is convenient to assume that the net magnetic flux associated with the entry-end effect wave in the interval $(2k-2)\tau_e \leq x \leq (2k-1)\tau_e$ must be equal to that in the interval $(2k-1)\tau_e \leq x < 2k\tau_e$ (see Fig. 1). Thus:

$$\begin{aligned}
\Phi_{e1} + \Phi_{e2} &= 0 \\
\Phi_{e3} + \Phi_{e4} &= 0 \\
&\vdots \\
\Phi_{e2p-1} + \Phi_{e2p} &= 0
\end{aligned} \qquad (7)$$

This assumed equality and the damped nature of the end effect wave implies that the space distribution of magnetic flux in the x direction cannot be sinusoidal. The analysis of higher space harmonics of a damped magnetic flux wave due to end effect would be complicated. Therefore, the following development considers a flux density distribution that is sinusoidal within each wavelength $2\tau_e$, but in which the amplitude is damped progressively from wavelength to wavelength. From equation (7) and the preceding equations for flux per pole, the following expressions arise:

$$\begin{aligned}
1 + e^{-\frac{\tau_e}{T_e}} &\neq e^{-\frac{\tau_e}{T_e}} + e^{-\frac{2\tau_e}{T_e}} \\
e^{-\frac{2\tau_e}{T_e}} + e^{-\frac{3\tau_e}{T_e}} &\neq e^{-\frac{3\tau_e}{T_e}} + e^{-\frac{4\tau_e}{T_e}} \\
&\vdots \\
e^{-\frac{(2p-2)\tau_e}{T_e}} + e^{-\frac{(2p-1)\tau_e}{T_e}} &\neq e^{-\frac{(2p-1)\tau_e}{T_e}} + e^{-\frac{2p\tau_e}{T_e}}
\end{aligned} \qquad (8)$$

These equations are clearly not mathematical equalities and are therefore inconsistent with the physical continuity of flux. To force consistency with flux continuity, the left and right hand sides are balanced, as follows:

$$\begin{aligned}
2e^{-\frac{\tau_e}{T_e}} &= 2e^{-\frac{\tau_e}{T_e}} \\
2e^{-\frac{3\tau_e}{T_e}} &= 2e^{-\frac{3\tau_e}{T_e}} \\
&\vdots \\
2e^{-\frac{(2p-1)\tau_e}{T_e}} &= 2e^{-\frac{(2p-1)\tau_e}{T_e}}
\end{aligned} \qquad (9)$$

This balancing is used to define the amplitude of each progressive wavelength of the damped end effect wave.

The instantaneous value of airgap EMF per phase induced by the end effect wave is then calculated as follows:

$$e_e = - \sum_{k=1}^{p} N_{pe}\, k_{we}\, \frac{d\Phi_{e2k-1}}{dt}$$

Putting $\Phi_{e2k-1} = \Phi_{e2k}$, gives:

$$e_e = - 2\pi f \frac{N}{p} \frac{\tau_e}{\tau} k_{we} \frac{L\, B_{me}}{\frac{1}{T_e^2} + \left(\frac{\pi}{\tau_e}\right)^2} \cdot f(\delta) \cdot \cos\omega t \cdot$$

$$2\left(e^{-\frac{\tau_e}{T_e}} + e^{-\frac{3\tau_e}{T_e}} + e^{-\frac{5\tau_e}{T_e}} + \ldots + e^{-\frac{(2p-1)\tau}{T_e}}\right) \quad (10)$$

where N_{pe} = number of turns per pole pair per phase for the end effect wave, k_{we} = winding factor for the end effect wave. The right hand side of equation (10) holds the geometric series in which the first term is $\exp(-\tau_e/T_e)$, the common ratio is $\exp(-2\tau_e/T_e)$ and the number of terms is p. Substituting the expression for sum of exponential terms in equation (10) yields:

$$e_e = - 2\pi f N k_{we} \frac{\tau_e}{\tau} \frac{L\, B_{me}}{\frac{1}{T_e^2} + \left(\frac{\pi}{\tau_e}\right)^2} \cdot f(\delta) \cdot 2e^{-\frac{p\tau_e}{T_e}} \cdot$$

$$\frac{\sinh\left(\frac{p\tau_e}{T_e}\right)}{p \sinh\left(\frac{\tau_e}{T_e}\right)} \cos\omega t = - E_{me} \cos\omega t \quad (11)$$

where E_{me} = peak value of airgap EMF due to end effect. The peak value of the magnetic flux density entry-end-effect wave is approximately equal to B_{ms}, i.e. $B_{me} \approx B_{ms}$ for x = 0. A precise computation of B_{me} would involve developing a complicated function which depends on the construction, operating conditions and phase unbalance of the LIM.

5. Total EMF Induced in Primary Winding, and End Effect Factor

According to equations (2), (3), (5), (6) and (11), and putting $B_{me} \approx B_{ms}$ at x = 0, the following expression for total EMF induced in the primary winding can be obtained:

$$e = - \sqrt{2}\, E_s \cos\omega t - \sqrt{2}\, E_s(-k_e)\cos\omega t$$

$$= - \sqrt{2}\, E_s(1 - k_e)\cos\omega t \quad (12)$$

where:

(i) the rms EMF due to the travelling field of amplitude B_{ms} is

$$E_s = \frac{2\pi}{\sqrt{2}} f N k_w \frac{2}{\pi} L\, \tau\, B_{ms} \quad (13)$$

(ii) the end effect factor then becomes:

$$k_e = - \frac{k_{we}}{k_w} \frac{\frac{\pi\tau_e}{\tau^2}}{\frac{1}{T_e^2} + \left(\frac{\pi}{\tau_e}\right)^2} f(\delta)\, e^{-\frac{p\tau_e}{T_e}} \frac{\sinh\left(\frac{p\tau_e}{T_e}\right)}{p \sinh\left(\frac{\tau_e}{T_e}\right)} \quad (14)$$

The developed expression (14) is the final form for the new longitudinal end effect factor which can be used in design of LIMs. The number of turns per pole pair per phase for the end effect wave is equal to:

$$N_{pe} = N_p \frac{\tau_e}{\tau} = \frac{N}{p} \frac{\tau_e}{\tau} \quad (15)$$

The winding factor for the end effect wave is determined in a similar manner to that for higher space harmonics of induction machines, i.e.

$$k_{we} = \frac{\sin\left(\frac{\tau}{\tau_e}\frac{\pi}{2m}\right)}{q \sin\left(\frac{\tau}{\tau_e}\frac{\pi}{2mq}\right)} \cdot \sin\left(\frac{\tau}{\tau_e}\frac{\pi}{2}\frac{w_c}{\tau}\right) \quad (16)$$

where q = number of slots per pole per phase, m = number of phases, and w_c = coil pitch.

The pole pitch τ_e and the attenuation constant T_e can be determined using the expressions given by Yamamura [1]:

$$\tau_e = \frac{2\pi}{D} \quad (17)$$

$$T_e = \frac{2gk_c}{Cgk_c - v\mu_o\sigma_{A\ell}d} \quad (18)$$

where

$$C = \frac{1}{\sqrt{2}}\sqrt{\sqrt{\left(\frac{\mu_o v \sigma_{A\ell} d}{k_c g}\right)^4 + 16\left(\frac{\omega\mu_o\sigma_{A\ell}d}{k_c g}\right)^2} + \left(\frac{\mu_o v\sigma_{A\ell}d}{k_c g}\right)^2} \quad (19)$$

$$D = \frac{1}{\sqrt{2}}\sqrt{\sqrt{\left(\frac{\mu_o v \sigma_{A\ell} d}{k_c g}\right)^4 + 16\left(\frac{\omega\mu_o\sigma_{A\ell}d}{k_c g}\right)^2} - \left(\frac{\mu_o v\sigma_{A\ell}d}{k_c g}\right)^2} \quad (20)$$

The formulae (18), (19), and (20) are valid for double-sided LIMs with aluminum secondary. The airgap thickness is g, the secondary thickness is d, the conductivity is $\sigma_{A\ell}$ and the Carter factor is k_c. For single-sided LIMs with a double layer secondary (aluminum and solid steel), $k_c(g + d)$ should be substituted for $k_c g$ and d_R' substituted for d, where d_R' is the equivalent thickness of the double-layer secondary for evaluating the eddy-current resistance. The equivalent thickness can be estimated from the electromagnetic field distribution in the secondary in a way similar to that used for the double-sided LIM [8].

6. Evaluation of the Angle δ

The angle δ between the magnetic flux density wave travelling with synchronous velocity and the end effect wave can be determined by the application of the following two boundary conditions:

(i) Under assumption (c), no end effect exists ($k_e = 0$) at $v = v_o$, where $0 \leq v_o < v_s$. Denoting $\delta = \delta_o$ for $k_e = 0$, equation (6) becomes:

$$\frac{1}{T_e} \sin\delta_o + \frac{\pi}{\tau_e} \cos\delta_o = 0 \qquad (21)$$

δ_o is therefore given by:

$$\delta_o = 180° - \tan^{-1} \left(\pi \frac{T_e}{\tau_e} \right)_{v=v_o} \qquad (22)$$

If $v_o = 0$, equations (17), (18), (19), (20), and (22) yield

$$\delta_o = 180° - \tan^{-1} (1) = 135° \qquad (23)$$

(ii) Using assumption (d), i.e. $B_{me} = B_{ms}$ for $T_e \to \infty$ and $\tau_e = \tau$, it can be shown, from equation (16), that $k_{we} = k_w$, and from equation (14) with:

$$\lim_{T_e \to \infty} e^{-\frac{p\tau_e}{T_e}} = 1 \quad \text{and} \quad \lim_{T_e \to \infty} \frac{\sinh \left(\frac{p\tau_e}{T_e} \right)}{p \sinh \left(\frac{\tau_e}{T_e} \right)} = 1$$

that the end effect factor becomes:

$$k_e = - \cos\delta \qquad (24)$$

To have total cancellation of the EMF due to the magnetic flux density travelling with synchronous velocity for this limiting condition, the end effect factor k_e should be equal to 1. From equation (19), this condition is satisfied when:

$$\delta = 180° \quad \text{if} \quad T_e \to \infty \quad \text{and} \quad k_e \to 1$$

Thus, the angle δ will be in the range $\delta_o \leq \delta \leq 180°$. In practice the highest synchronous speed is likely to be about 150 m/s. At this speed, the angle δ is assumed to be 180° ($k_e = 1$). Hence, we postulate that the angle δ can be approximated by the following function:

$$\delta \approx \delta_o + c\, v_e \qquad (25)$$

where δ_o is given by equation (22), and the constant c is equal to:

$$c \approx \frac{1}{150} \tan^{-1} \left(\pi \frac{T_e}{\tau_e} \right)_{v=v_o} \qquad (26)$$

and

$$v_e = \frac{v - v_o}{v_s - v_o} v_s \qquad \text{for } v \geq v_o$$

$$v_e = 0 \qquad \text{for } v \leq v_o$$

Test data indicates that $v_o \approx 0.5\, v_s$ for very high speed LIMs ($v_s \approx 150$ m/s), i.e. $k_e = 0$ for $v = v_o$.

7. Equivalent Circuit Including Longitudinal End Effect

The equivalent circuit of the LIM with longitudinal end effect included is shown in Fig. 2. The impedance Z_e is equal to:

$$Z_e = \frac{1 - k_e}{k_e} Z_{tot} \qquad (27)$$

where

$$Z_{tot} = \frac{Z_g \cdot Z'_{sec}}{Z_g + Z'_{sec}} \qquad (28)$$

The airgap (mutual) impedance is Z_g, and the secondary impedance referred to the primary winding is Z_{sec}'. The end effect impedance Z_e tends to infinity as the end effect factor tends to zero (at $s = 1$). The rms EMF calculated from the equivalent circuit is:

$$E = I \frac{Z_e Z_{tot}}{Z_e + Z_{tot}} = (1 - k_e) E_s \qquad (29)$$

where

$$E_s = I Z_{tot} \qquad (30)$$

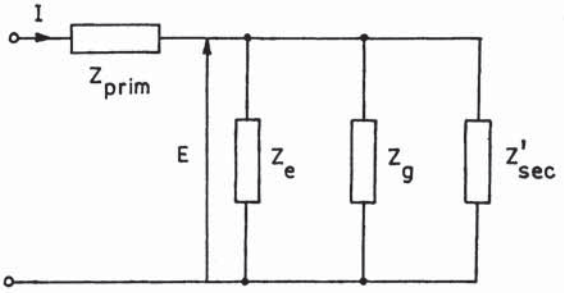

Fig. 2 Equivalent circuit with end effect taken into account: Z_{prim} = impedance of primary; Z_{sec}' = impedance of secondary referred to primary; Z_g = mutual impedance; Z_e = end effect impedance; I = primary current; and E = airgap EMF

8. Comparison of Analysis with Measurement

To validate the analytical expression for longitudinal end effect factor (14), the computed performance has been compared with experimental results from two large-scale single-sided LIMs, one tested at the Canadian Institute of Guided Ground Transport (CIGGT) at Queen's University [5,6,9] and one tested by General Electric Company [10]. Both test facilities use rotating wheels to provide relative motion between

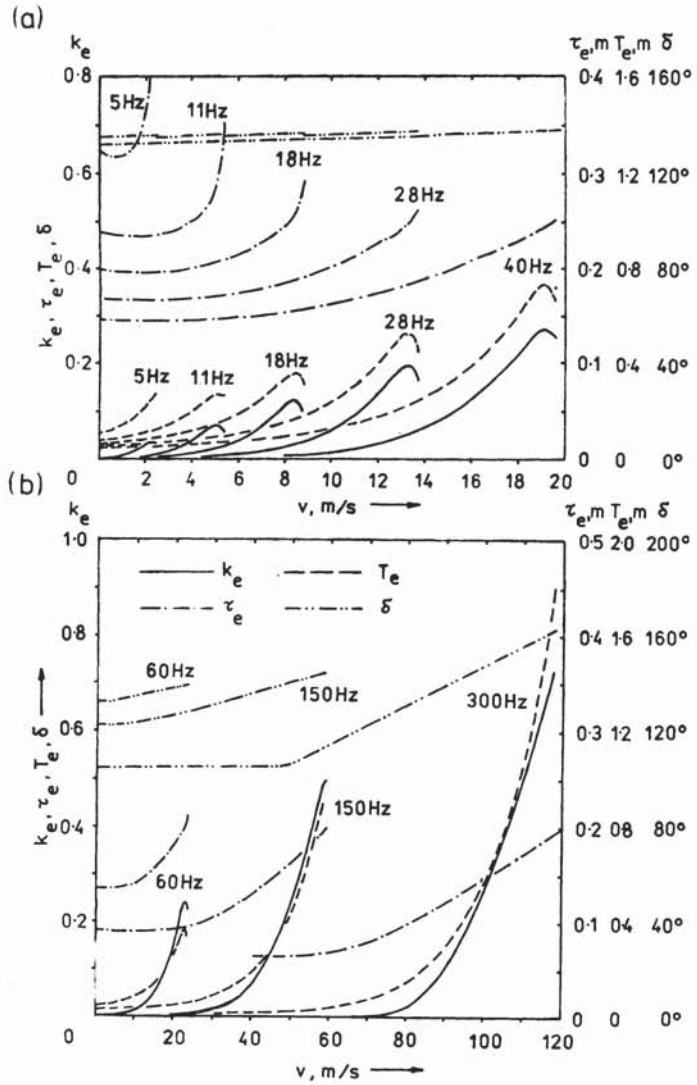

Fig. 3 Parameters k_e, τ_e, T_e and δ versus speed at constant frequencies and constant current excitation (I = 200 A): (a) CIGGT LIM; (b) GEC LIM

rim-mounted guideway components (solid steel with aluminum cap) and a stationary vehicle module (the LIM primary). Design data for the LIMs, used as input parameters for performance computation, are as follows:

	CIGGT LIM	GEC LIM
Number of phases, m	3	3
Number of pole pairs, p	3	2
Nominal input current, I	200 A	200 A
Number of primary series turns per phase, N	108	48
Primary coil pitch, w_c	0.1944 m	0.1557 m
Width of primary stack, L	0.101 m	0.1715 m
Pole pitch, τ	0.25 m	0.20 m
Nominal airgap, g	15 mm	18.2 mm
Number of slots per pole per phase, q	3	3
Secondary width (back iron), w	0.111 m	0.1715 m
Width of aluminum cap	0.179 m	0.2985 m
Thickness of back iron, h_{sec}	25.4 mm	47.37 mm
Thickness of aluminum cap, d	2.5 mm	3.175 mm

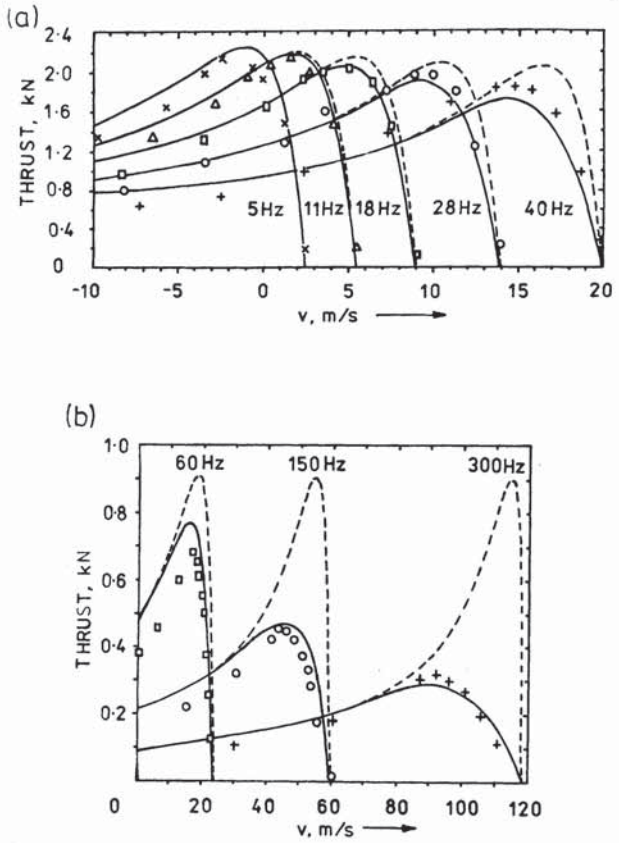

Fig. 4 Thrust versus speed at constant frequency and constant current excitation (I = 200 A); calculations according to the authors method: (a) CIGGT LIM (b) GEC LIM

- - - - - calculations without end effect
--------- calculations with end effect
+ + + 40 Hz and 300 Hz
° ° ° 28 Hz and 150 Hz
□ □ □ 18 Hz and 60 Hz } experimental results
Δ Δ Δ 11 Hz
x x x 5 Hz

The performance of the LIMs has been calculated for constant current excitation I = 200 A at input frequencies from 5 Hz to 300 Hz, for comparison with test results. For the computer program, the two-dimensional, four layer model (airgap, aluminum, solid steel and air) has been used [11]. This includes variable magnetic permeability, hysteresis losses in the solid steel secondary core, power loss in the primary stack, saturation of the magnetic circuit, transverse edge effect, and longitudinal end effect according to Sections 5, 6 and 7. In accordance with discussion in Section 6, we take $v_o = a\, v_s$, where $0 \leq a < 1$. For both LIMs, $a = 0.5\, v_s / 150$, with synchronous speed in m/s. The calculated end effect factor k_e (14), the pole pitch τ_e (17), the attenuation constant T_e, equation (18), and the angle δ (26) are plotted as functions of speed in Fig. 3.

Thrust versus speed curves, are presented in Fig. 4. Thrust calculations including the end effect are seen to be closer to test results than those obtained without end effect. For low velocities, i.e. for input frequency f < 18 Hz, the influence of end effect on the thrust is negligibly small.

As far as the authors are aware, three different T-type equivalent circuits which include an end effect factor have been presented in the literature [2,3,12]. The circuits given by [2,12] are related to double-sided LIMs, and assume the secondary reactance to be zero. This assumption precludes a realistic comparison of these methods with the method presented in this paper. Only the method [3] by Nonaka and Higuchi contains the full equivalent circuit (primary resistance and reactance, magnetizing reactance, secondary resistance and reactance) for the single-sided LIM. These authors introduce two longitudinal end effect factors k_{e1} ≤ for $Re[Z_{tot}]$ and k_{e2} for $Im[Z_{tot}]$, where $k_{e1} < k_{e2}$.

Comparison of thrust-velocity curves obtained from Nonaka and Higuchi's method [3] with the test results is shown in Fig. 5. Figures 4 and 5 show that both methods predict the same behaviour of thrust due to the end effect, and give very similar results for input frequencies of 5 Hz and 11 Hz, i.e. for low speeds at which the end effect is negligibly small. For higher frequencies and speeds, the method proposed by the authors gives better results. The authors method is also simpler (one end effect factor rather than two) than that of Nonaka and Higuchi [3].

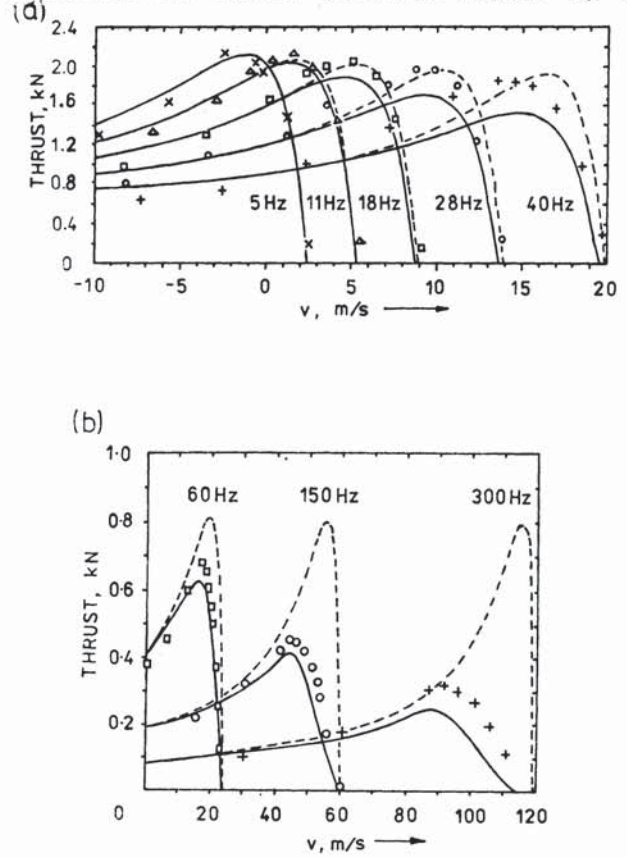

Fig. 5 Thrust versus speed at constant frequency and constant current excitation (I = 200 A); calculations according to Nonaka and Higuchi's method [3]: (a) CIGGT LIM (b) GEC LIM

- - - - - calculations without end effect
--------- calculations with end effect
+ + + 40 Hz and 300 Hz
° ° ° 28 Hz and 150 Hz
□ □ □ 18 Hz and 60 Hz
Δ Δ Δ 11 Hz
x x x 5 Hz
} experimental results

9. Conclusions

The method of accounting for the longitudinal end effect, as presented here, is considered to be sufficiently accurate for the investigation and design of LIMs. The equivalent circuit, Fig. 3, including end effect, is simpler than those previously proposed [2,3,12]. The end effect factor, according to expression (14), depends on the number of pole pairs p, the angle δ between the magnetic flux density wave travelling with synchronous velocity and the entry-end-effect wave, the pole pitch τ, and the pole pitch τ_e and attenuation constant T_e of the end effect wave. It should be noted that, in developing the end effect factor, we have not considered exit end effects. However, longitudinal exit end effects, in general, produce much less degradation in LIM performance than longitudinal entry end effects [1] and can reasonably be neglected.

10. Acknowledgements

This work was supported by the Natural Sciences and Engineering Research Council (NSERC) of Canada, and one of the authors (J.F.G.) is indebted to NSERC for an International Scientific Exchange Award to conduct research at Queen's University for the year 1983/84.

11. References

1. Yamamura, S., "Theory of Linear Induction Motors", University of Tokyo Press, 1972.
2. Hirasa, T., Ishikawa, S., and Yamamuro, T., "Equivalent Circuit of Linear Induction Motors with End Effect Taken into Account", Electrical Engineering in Japan, Vol. 100, No. 2, 1980, pp. 65 - 71.
3. Nonaka, S., and Higuchi, T., "Approximate Equations for Calculation of Characteristics of Single-Sided Linear Induction Motors", Electrical Engineering in Japan, Vol. 102, No. 5, 1982, pp. 18 - 25.
4. Nasar, S. A. and Boldea, I., "Linear Motion Electric Machines", John Wiley & Sons, 1976.
5. Dawson, G. E., and Eastham, A. R., "The Comparative Performance of Single-Sided Linear Induction Motors with Squirrel-Cage, Solid-Steel and Aluminum-Capped Reaction Rail", 16th Annual IEEE Industry Applications Society Meeting, Philadelphia, IEEE Conference Record 81CH1678-2, October 1981, pp. 323 - 329.
6. Eastham, A. R., Dawson, G. E., Pringle, D. M., and Davidson, J. A., "Comparative Experimental Evaluation of the Performance of a SLIM with a Solid-Steel Reaction Rail and with an Aluminum-Capped Reaction Rail", CIGGT Report No. 80-7, Queen's University, Kingston, 1980.

7. Gieras, J. F., "Equipment for Testing Single-Sided Flat Linear Induction Machines" (In Polish), Przegląd Elektrotechniczny (Electrotechnical Review), No. 3, 1984, pp. 84 - 89.
8. Gieras, J. F., "Simplified Theory of Double-Sided Linear Induction Motor with Squirrel Cage Electric Secondary", Proc. IEE, Part B, Vol. 130, No. 6, 1983, pp. 424 - 430.
9. Eastham, A. R., Dawson, G. E., Atherton, D. L., and Schwalm, C. L., "Test Facility for the Determination of Linear Induction Motor Performance", CIGGT Report No. 80-6, Queen's University, Kingston, 1980.
10. Kliman, G. B., Mischler, W. R., and Oney, W. R., "Performance of a Single-Sided Linear Induction Motor with Solid Back Iron and with Various Misalignments", Report No. FRA/ORD-80/53-1, GEC, Schenectady, New York, 1980.
11. Gieras, J. F., Eastham, A. R., and Dawson, G. E., "The Influence of Secondary Solid Ferromagnetic Plate Thickness on the Performance of Single-Sided Linear Induction Motors", Electric Machines and Power Systems, Vol. 10, 1985, pp. 67-77.
12. Matsumiya, T., and Takagi, K., "End Effect and Equivalent Circuit of Linear Induction Machines", Electrical Engineering in Japan, Vol. 21, No. 1, 1971, pp. 117 - 127.

JACEK F. GIERAS (M'83) was born in [redacted]. He received the M.Sc. (Mgr inż.) degree in Electrical Engineering from the Technical University of Łódź, the Ph.D.(Dr inż.) and D.Sc. (Dr hab.) degrees from the Technical University of Poznań (Poland) in 1971, 1975 and 1980 respectively. His research activities include analysis of electromagnetic fields in electrical machines and devices, computer-aided-design of electrical machines, magnetic levitation, and industrial drives. At present, he is a Visiting Associate Professor at Queen's University. He is the co-author of monography "Induction machines with solid rotor" issued by the Polish Scientific Publishing House (Warszawa-Poznań) in 1977, author of a textbook "Special Purpose Electric Machines" (ATR Bydgoszcz, 1983) and author of 65 scientific papers published in Poland, Great Britain, USA, India, West and East Germany, Switzerland, Czechoslovakia and Hungary. He holds four Polish patents.

GRAHAM E. DAWSON (S'66, M'69) was born in North Vancouver, British Columbia on November 11, 1939. He received his B.A.Sc., M.A.Sc., and Ph.D. degrees from the University of British Columbia in 1963, 1966 and 1970 respectively. In 1969 he joined the Department of Electrical Engineering, Queen's University at Kingston as an assistant professor. He was promoted to Associate Professor in 1975 and to Professor in 1981. His electrical engineering research activities have been associated with the transportation industry where he has current interest in the design and performance of rotary and linear traction motors and energy management of transportation systems. He is a registered professional engineer in the Province of Ontario and a member of the Canadian Society for Electrical Engineering.

ANTHONY R. EASTHAM (M'75, SM'83) received the B.Sc. degree in Physics from the University of London in 1965, and the Ph.D. degree from the University of Surrey in 1969. After research work at Plessey Telecommunications Ltd. and at the University of Warwick, he joined the Canadian Institute of Guided Ground Transport where he coordinated a group that technically defined, component tested and assessed high-speed Maglev in Canada. Dr. Eastham is now a professor of electrical engineering at Queen's University in Kingston, Ontario, having joined the faculty in 1978. His research activities include innovative urban and high-speed transportation, linear electric drives, and electromagnetic analysis. Dr. Eastham is a Registered Professional Engineer of the Province of Ontario.